5
Removal of Uranium from Waste Water

This chapter describes about application of surface fluorinated hematite (F-α-Fe_2O_3) for uranium removal from waste water. The sorption of U(VI) from aqueous solution was investigated as a function of pH, contact time and concentration using batch technique. The adsorption capacity (q_m) was found to be 79 mg/g using Langmuir adsorption isotherm and the equilibrium was achieved within one hour. The isotherm data shows better fit with Langmuir than Freundlich equations and follow the pseudo-second-order kinetic model. These results are best with maximum adsorption capacity of any hematite/modified hematite material. The chapter is composed of four sections and eleven sub-sections. The introduction of chapter is discussed in section 5.1. The results and discussion of physicochemical characterization techniques are explained in the section 5.2. Adsorption experiments are detailed in section 5.3. The concluding remark is placed in section 5.4.

5.1 INTRODUCTION

Uranium is a hazardous heavy metal, due to its high chemical toxicity and radioactivity. Ingestion of Uranium causes severe liver and kidney damage that could lead to even death (Schematic Figure 5.1).

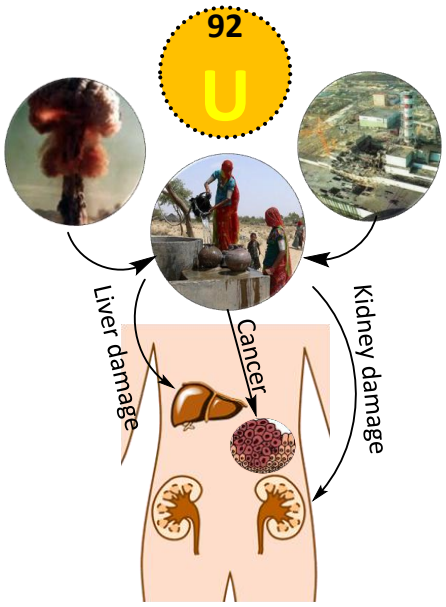

Figure 5.1: Uranium contamination and toxicity

The World Health Organization (WHO) has determined that U(VI) is a human carcinogen with maximum concentration 30 ppb in water [WHO, 2017; Ilaiyaraja et al., 2013]. According to U.S. Environmental Protection Agency (EPA), Maximum Contamination Level (MCL) for uranium is 30 ppb total uranium or 15 pCi/L gross alpha.[US Environmental Protection Agency, 2018]. Uranium has five oxidation states ranging from +2 to +6, among them

U(IV) and U(VI) are the most common. Uranium (IV) sparingly dissolve in the water, whereas uranium (VI) is highly soluble.

Uranium enters into the environment through the activities associated with the nuclear industry, milling, mining, waste disposal, nuclear accident and nuclear explosion [Bargar et al., 2000; Simon et al., 2008]. The high solubility of U(VI) is pertain to the formation of the stable linear uranyl ion, UO_2^{2+} and related hydrolyzed species such as UO_2OH^+, $UO_2(OH)_2$, and $(UO_2)_2(OH)_2^{2+}$ [Duff and Amrhein, 1994]. Due to serious environmental toxicity, removal of uranium from aquatic ecosystem has been concern and various processes such as chemical precipitation, ion exchange, evaporation, coagulation, membrane separation and adsorption have been developed [Chanda and Rampel, 1992; Duff and Amrhein, 1994; Gu et al., 1998; Ho and Doern, 1985; Raff and Wilken, 1999]. Among these methods, adsorption has been established as an effective and convenient technique due to selectivity, ease of operation, efficiency, low cost and controllable solution chemistry of adsorbent.

A variety of adsorbents such as organic [Abdi et al., 2017; Yi et al., 2017], inorganic [Chen et al., 2018; Kuncham et al., 2017; S Yang et al., 2017], carbon based material [Saleh et al., 2017; Stafiej and Pyrzynska, 2007], bio-sorbent [Wang et al., 2009; WM Youssef, 2017] have been developed for uranium removal. Out of them, solid inorganic adsorbents have significant operational and separation advantages.

Despite cost effectiveness, wide availability and low toxicity with high chemical affinity towards toxicants, limited studies have been carried out towards iron oxide [Benjamin et al., 1996]. Geologically, Iron oxides are common components of soil with important sedimentation characteristics [Duff et al., 2002]. Based on synthetic processes and morphologies hematite shows variable uranium adsorption characteristics i.e. Shuibo *et al.* prepared hematite by hydrolyzing ferric chloride which gave maximum adsorption capacity (q_m) of 3.54 mg/g at pH 7 [Shuibo et al., 2009] while hematite synthesized from ferric oxide with peanut-like morphology takes 5 hr. equilibrium time at acidic pH with moderate uranium uptake [Zhao et al., 2012]. Spherical hematite particles prepared via sol-gel method shows low uranium adsorption in combination with other metals [Murphy et al., 1999]. Uranium(VI) sorption to hematite in the presence of humic acid has been reported with higher adsorption at low pH values [Lenhart and Honeyman, 1999].

Even though various advantages, hematite has not been used for practical applications due to its low q_m and long kinetic equilibrium time (> 5h). Therefore, this study deals with investigation of various surface fluorinated α-Fe_2O_3 for uranium sorption. The fluorinated hematite (F-α-Fe_2O_3) was prepared using single pot hydrothermal method, as described in material synthesis and characterization chapter and used for adsorption studies. F-TEDA was used as fluorinating agent and four F-α-Fe_2O_3 samples prepared using varying quantity of F-TEDA (10% wt. to 40% wt.)

5.2 PHYSICOCHEMICAL CHARACTERIZATION

Physicochemical characterizations of the materials were performed for confirming the uranium adsorption on fluorinated hematite, surface area analysis and estimation of Uranium in contaminated and decontaminated aqueous solution. The characterization techniques and their analysis are presented in subsequent sub-sections from 5.2.1 to 5.2.6 in systematic manner as followings:

(5.2.1) *Fourier Transform Infrared Spectra* was used to find out the associated peaks of uranium adsorbed onto hematite.

(5.2.2) *X-ray Diffraction* was performed for identifying the crystallographic phase.

(5.2.3) *X-ray Photo Electron Spectra* (*XPS)* were recorded for determining elemental composition before and after adsorption.

(5.2.4) *FESEM Imaging and EDS* were carried out for establishing morphology and composition.
(5.2.5) *BET Surface Area Analyzer* was used for measuring surface area and related properties.
(5.2.6) *Inductively Coupled Plasma Optical Emission Spectrophotometer (ICP-OES)* was utilized for trace element (Uranium) analysis in aqueous medium.

5.2.1 Fourier Transform Infrared Spectra Analysis

In order to establish the presence of uranium due to sorption, FTIR spectra of F-α-Fe_2O_3 and uranium adsorbed F-α-Fe_2O_3 were recorded in the range of 4000 cm^{-1} to 400 cm^{-1}[Salama et al., 2015]. The FTIR spectra of F-α-Fe_2O_3 and Uranium adsorbed F-α-Fe_2O_3 are represented in Figure 5.2. The bands observed at 471 cm^{-1} and 544 cm^{-1} can be attributed to metal oxygen stretching vibration modes of hematite. Whereas, in case of uranium adsorbed on F-α-Fe_2O_3, the peak at 911 cm^{-1} represents uranyl oxide peak, otherwise absent in F-α-Fe_2O_3, and may be assigned to the antisymmetric vibration of the $[O= U^{VI}=O]^{2+}$ group [Amayri et al., 2004]. However, the symmetric stretching vibration of the uranyl cation [$v_1(UO_2^{2+})$] is inactive. An absorption band of uranyl (VI) ion is also seen at 696 cm^{-1} which is absent in the spectrum of F-α-Fe_2O_3 [Anirudhan et al., 2010].

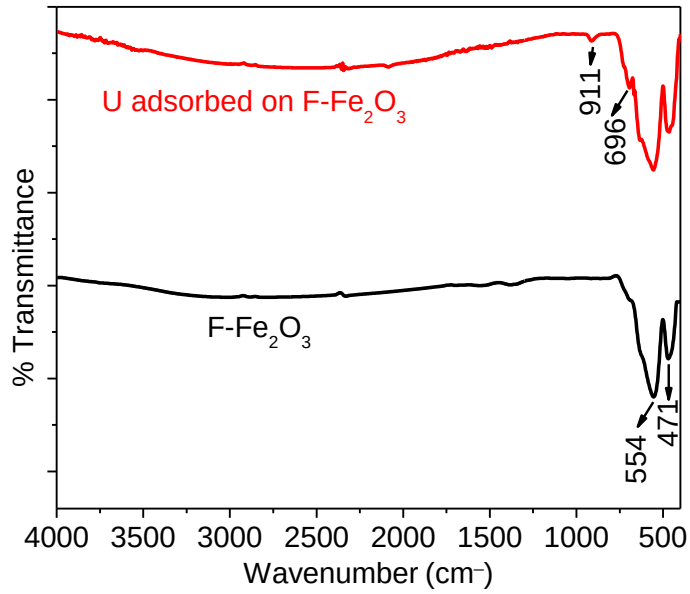

Figure 5.2: FTIR spectra of F-α-$Fe_2O_3$and Uranium adsorbed F-α-Fe_2O_3

5.2.2 X-ray Diffraction Analysis

X-ray pattern were recorded in 20° to 80° 2θ range to identify the crystallographic phase. The diffraction patterns are shown in Figure 5.3. XRD patterns of F-α-Fe_2O_3 (prepared by using 30 wt% of F-TEDA) showed rhombohedra structure of hematite (JCPDS data card number 86–0550) with crystallite size of 35 nm as calculated by Scherrer's equation. After adsorption of U(VI) onto F-α-Fe_2O_3 the 2θ values shows negligible change in their position and the appearance which indicates no crystallization of uranium oxides on F-α-Fe_2O_3.[Zalkind et al., 2017].

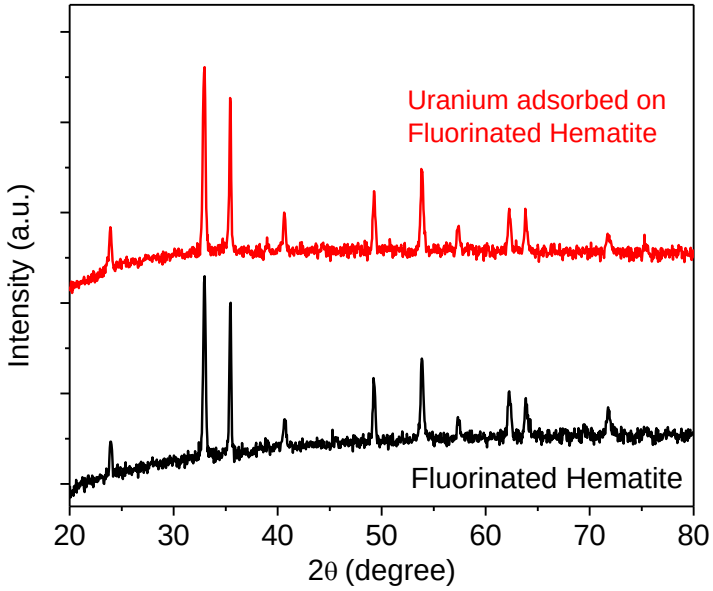

Figure 5.3: X-ray diffraction patterns of F-α-Fe_2O_3 and U(VI)-F-α-Fe_2O_3

5.2.4 X-ray Photo Electron Spectra

In order to study the sorption of U(VI) onto F-α-Fe_2O_3, XPS spectra were recorded before and after sorption of U(VI). The survey spectra are demonstrated in Figure 5.4. It shows C 1s, O 1s, F 1s, and U 4f with characteristic doublet peaks of U $4f_{5/2}$ and U $4f_{7/2}$.

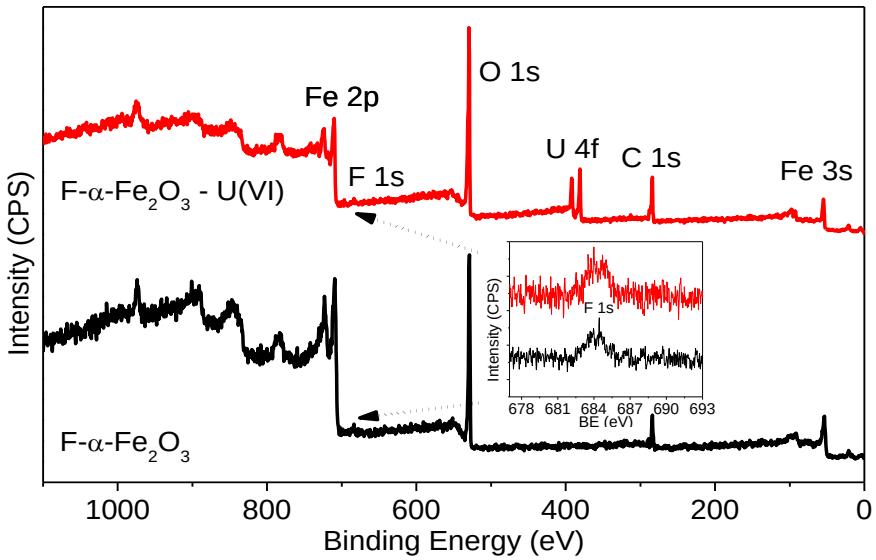

Figure 5.4: XPS spectra of spectra of F-α-Fe2O3 before and after U(VI) adsorption, survey XPS

The high resolution spectrum of U 4f is present in Figure 5.5a. The peaks at 392.5 eV and 381.7 eV are assigned to the U $4f_{5/2}$ and $4f_{7/2}$ spin states, respectively [López et al., 2017]. The chemical shift of U $4f_{7/2}$ at 381.7 eV is indicative of U^{+6}. However, the U^{4+} peak between 380.2-380.7 eV which is associated with U $4f_{7/2}$ were not detected [Schindler et al., 2009a].The presence of $4f_{7/2}$ peak and its position at 381.7 eV confirms that the adsorbed U is in the oxidation state of U(VI) and no reduced state of U(IV) is occurring [Ilton and Bagus, 2011]. The peaks at 530.6 and 529.1 eV (Figure 5.5b) in the high resolution indicate O 1s profile of adsorbent, which represent the oxygen from hydroxyl groups bonded with metals and crystal lattice oxygen respectively [Schindler et al., 2009b]. After the adsorption, intensity of the metal-bonded oxygen has increased and it attributed to the uptake of the various uranyl bonded oxygen. However, no

separate O 1s peak observed for uranyl as the binding energies of O^{2-} and OH^- bands in O 1s spectra of iron compound are similar to those of uranyl [Sunder et al., 1996]. Furthermore, the shift in the binding energies of O 1s before and after U(VI) loading indicated that U(VI) sorption onto F-α-Fe_2O_3 occurred by complexation of oxygen [Mishra et al., 2015].

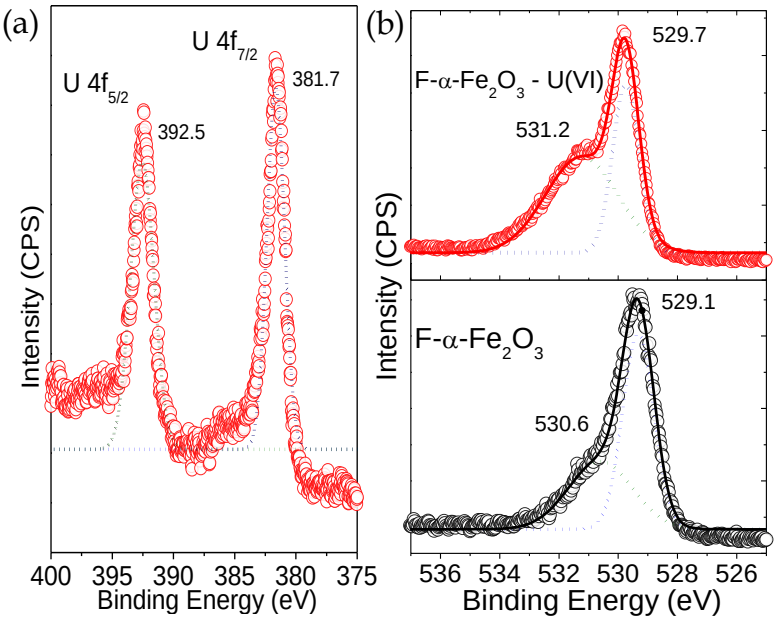

Figure 5.5: XPS spectra of spectra of F-α-Fe_2O_3 before and after U(VI) adsorption (a) high resolution of U 4f, and (b) high resolution of O 1s. The peaks are referenced to the C 1s line of adventitious hydrocarbon at 284.8 eV

5.2.4 FESEM Imaging and EDS Analysis

Figure 5.6a shows the field emission scanning electron micrograph (FESEM) of F-α-Fe_2O_3 powder (30% wt. of F-TEDA) after adsorption of uranium ions which exhibits loose aggregates of the particles.

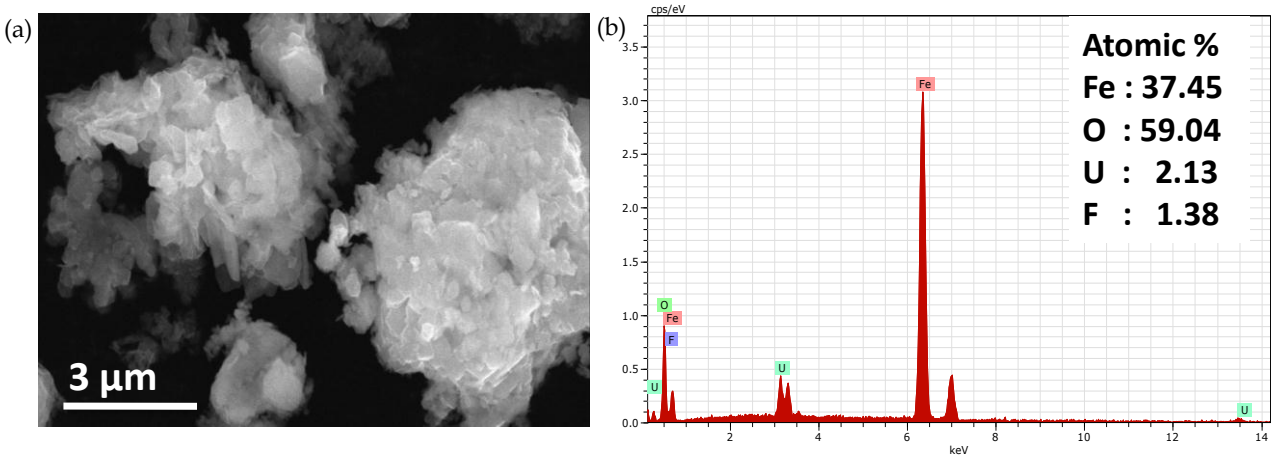

Figure 5.6: (a) FESEM image and (b) EDX profile of F-α-Fe_2O_3 - U(VI)

Figure 5.6b shows the presence of U(VI) on the surface of F-α-Fe_2O_3 powder which indicates that the powder has adsorption ability for removal of U(VI) ions from aqueous solutions.

5.2.5 BET Surface Area Analysis

The nitrogen adsorption-desorption isotherms are shown in Figure 5.7a-e. The specific surface areas were measured as 5.0-41.2 m^2/g by multi point Brunauer-Emmett-Teller (BET)

method for pristine α-Fe_2O_3 and fluorinated α-Fe_2O_3. The surface area and pore size data are summarized in Table 5.1.

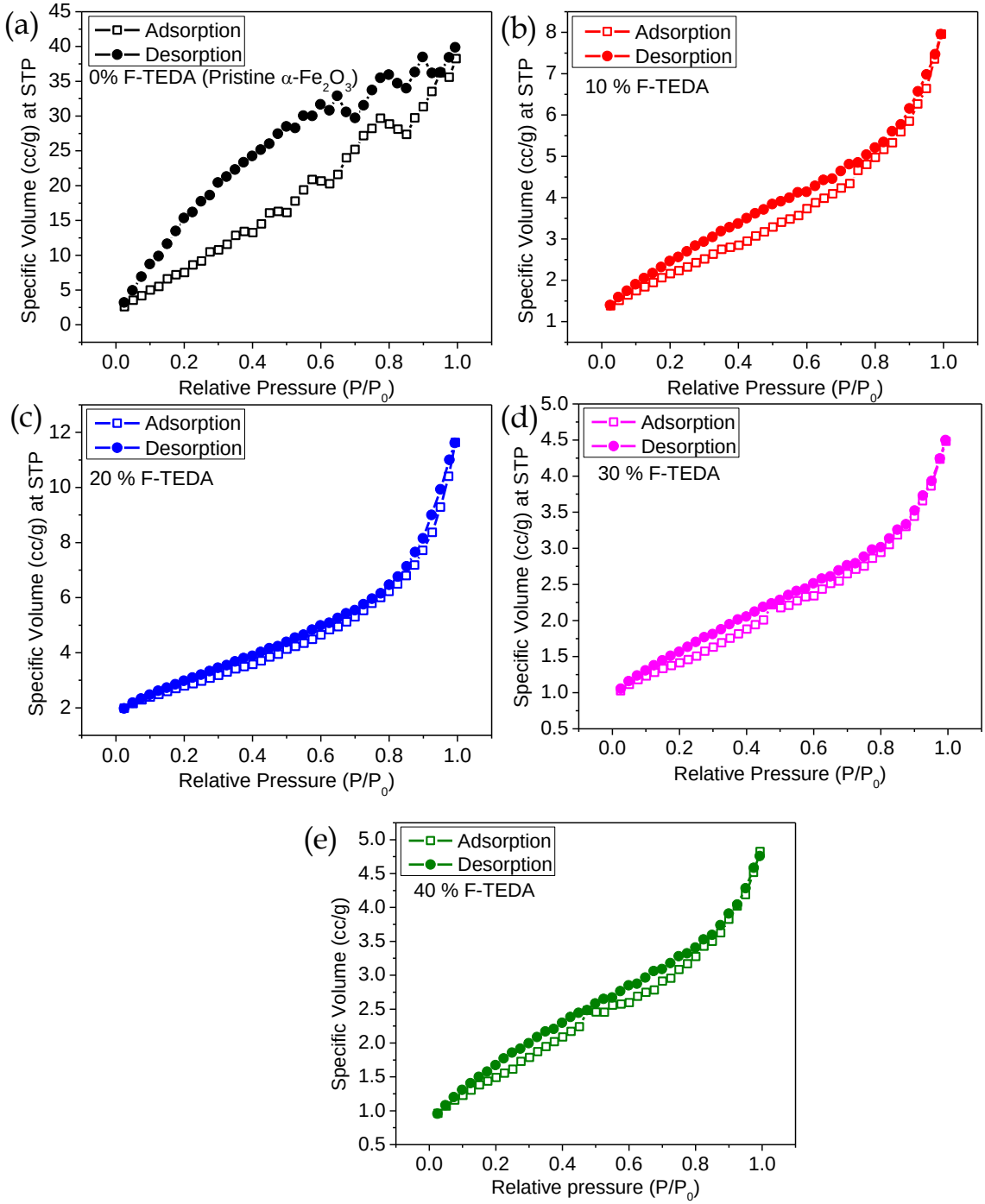

Figure 5.7: Nitrogen adsorption - desorption isotherms of (a) pristine α-Fe_2O_3 (b) 10% F-TEDA- F-α-Fe_2O_3 (c) 20% F-TEDA- F-α-Fe_2O_3 (d) 30% F-TEDA- F-α-Fe_2O_3 (e) 40% F-TEDA- F-α-Fe_2O_3

Table 5.1: Surface area and pore size of α-Fe_2O_3 and F-α-Fe_2O_3

SNo.	*Sample*	*Surface Area, m^2g^{-1}*	*Pore Size (radius), Å*
1.	Pristine α-Fe_2O_3	41.2	28.7
2.	10% F- α-Fe_2O_3	7.9	30.9
3.	20% F- α-Fe_2O_3	9.8	36.0
4.	30% F- α-Fe_2O_3	5.00	27.7
5.	40% F- α-Fe_2O_3	5.61	26.6

Surface area decreases consistently upon fluorination due to the symmetric growth of α-Fe_2O_3 in all directions. Although the surface area is decreasing however the the pore size of hematite and fluorinated hematite were within narrow distribution.

5.2.6 Inductively Coupled Plasma Optical Emission Spectrophotometer (ICP-OES) Analysis

The trace quantity of uranium in aqueous solution, before and after adsorption was estimated by ICP-OES. The instrument was calibrated using 18.2 MΩ cm DI water as blank and 25 ppm, 50 ppm and 100 ppm standard solution of uranium. The calibration curve is presented in Figure 5.8. The rho value was within acceptable limit (0.995).

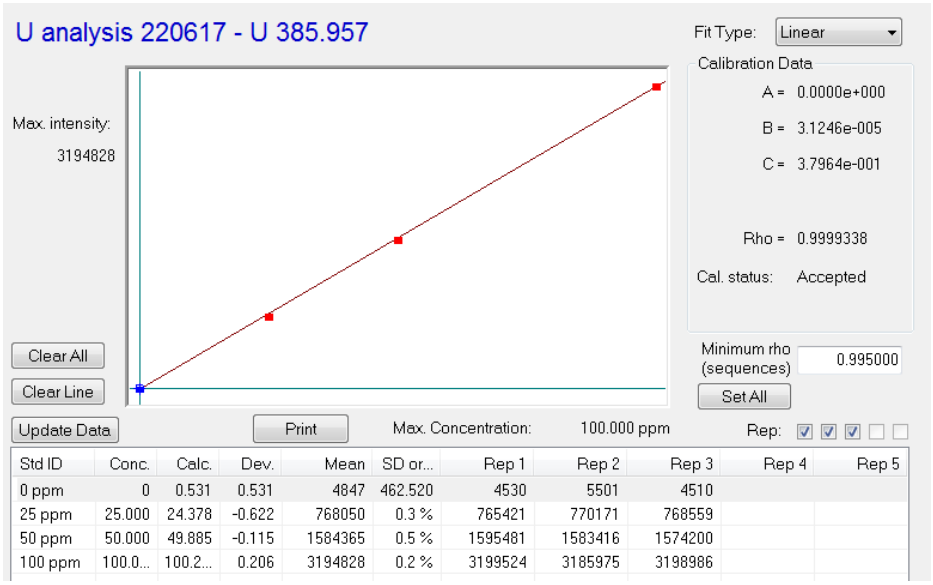

Figure 5.8: Calibration of ICP OES for uranium detection

5.3 BATCH ADSORPTION EXPERIMENTS

The objective of this study was to investigate the efficiency of surface fluorinated hematite (adsorbent) for uranium (adsorbate) removal from waste water by batch adsorption method. Uranium stock solution (1000 ppm) was prepared from uranylnitrate $UO_2(NO_3)_2.6H_2O$ as a source of U(VI) ions. The uranium running solutions were diluted from the stock solution to different multiple as per the requirement. All batch experiments were carried out by mixing 25 mg of adsorbent to 50 mL U(VI) solution under stirring at 140 rpm and at room temperature. In all adsorption experiments, pH of the system was adjusted at 5 by adding small volumes of diluted acid or base solution except those of pH segment. After attaining adsorption equilibrium the adsorbent was separated from the solution by 0.22 µm syringe filter. The uranium concentration in the filtrate was measured by ICP OES at 385.957 nm wave length in axial mode viewing of plasma for 15 seconds. The uranium adsorbed at the time t (q_t), adsorption capacity at equilibrium (q_e) and adsorption efficiency (% removal) at equilibrium was calculated according to the following equations:

$$q_t = \left(\frac{C_0 - C_t}{m}\right) \times V \quad (5.1)$$

$$q_e = \left(\frac{C_0 - C_e}{m}\right) \times V \quad (5.2)$$

$$\%\ Removal = \left(\frac{C_0 - C_e}{C_0}\right) \times 100 \quad (5.3)$$

Where, C_0 is the initial concentration of uranium (ppm), C_t is the concentration of uranium at time t (ppm), C_e is concentration of uranium at equilibrium (ppm), V is volume of solution in mL, and m is the mass of adsorbent added in mg.

The adsorption behavior and process were explored by fitting adsorption isotherms and kinetic models respectively. Further detailed study of batch adsorption experiments are discussed in subsequent sub sections from 5.3.1 to 5.3.5.

(5.3.1) *Effect of pH*
(5.3.2) *Effect of Fluorination on U(VI) Adsorption*
(5.3.3) *Effect of the Initial Concentration of the U(VI) Ions*
(5.3.4) *Effect of Contact Time (Adsorption Kinetics)*
(5.3.5) *Adsorption Isotherm*

5.3.1 Effect of pH

The effect of pH on the adsorption of U(VI) ions at equilibrium (3 h) was studied at room temperature in a pH range of 2-7 at 50 ppm. The solution of pH was adjusted to the desired value by adding 1N, 0.1N, 0.01N NaOH and 1N, 0.1N, 0.01N HCl standardized solutions. The speciation of uranium is affected by pH of the initial solution. Therefore, pH of the aqueous solution is an important parameter in the adsorption process. Figure 5.9 shows the dependence of the amount of uranium adsorbed on the equilibrium concentration of uranium at various pH.

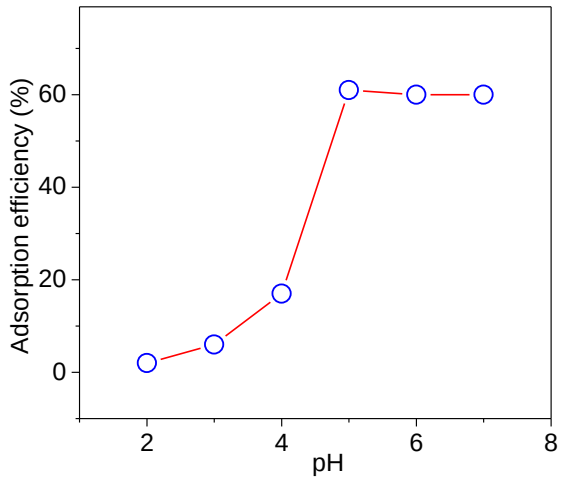

Figure 5.9: The effect of initial solution pH on U(VI) removal at 50 ppm concentration; volume, 50 mL; adsorbent dose, 25 mg; pH value, 2, 3, 4, 5, 6, 7; contact time, 60 min; temperature, 25 °C; rotating speed, 140 rpm

It is observed that the higher adsorption capacity for U(VI) ions was achieved at less acidic pH value. The adsorption capacity increases with the increase of the solution pH values in the pH ranges of 5-6. The maximum efficiency was achieved at pH 5. At lower pH range, up to pH 3, free UO_2^{2+} is predominant in solution and the adsorbed H^+ ions on the surface of F-α-Fe_2O_3 cause a strong electrostatic repulsion to U(VI) ions resulting into low adsorption. However, in the pH range of ≥ 4 to 6.5, positively charged solution species $(UO_2)_3(OH)^{5+}$ and $(UO_2)_4(OH)^{7+}$ successively becomes the dominant U(VI) species and are responsible for adsorption in CO_2-equilibrated systems.[Catalano and Brown, 2005] At pH ≥ 4 to 6.5, fluorine and oxygen becomes main existing form of F-α-Fe_2O_3 to attract uranyl ion through electrostatic attraction. The presence of surface fluorine increases surface potential of α-Fe_2O_3 which could substantiate strong surface electrostatic attraction towards U(VI) species at low pH.[Lu et al., 2019] However, The increased adsorption at pH 7 may be attributed to sorption of positive species as well as precipitation of schoepite.[Zeng et al., 2009]

5.3.2 Effect of Fluorination on U(VI) Adsorption

The effect of fluorine content, in F-α-Fe_2O_3 samples, on U(VI) ion adsorption was determined at 50 ppm U(VI) ion concentration using batch method. The comparative study to

elucidate effect of fluorine content in F-α-Fe_2O_3 (10% - 40% samples) on uranium adsorption is presented in Figure 5.10.

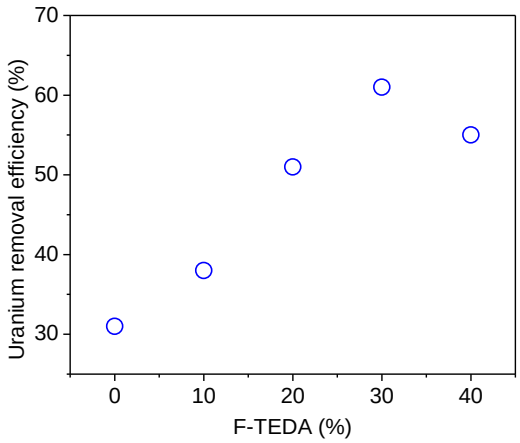

Figure 5.10: The effect of fluorination on U(VI) removal at 50 ppm concentration; volume, 50 mL; adsorbent dose, 25 mg; pH value 5, contact time, 60 min; temperature, 25 °C; rotating speed, 140 rpm

The removal efficiency corresponds to the content of fluorine in F-α-Fe_2O_3. The removal efficiency gradually increases from 31% in pristine to maximum 62% in 30% F-α-Fe_2O_3 and decline further for 40% F-α-Fe_2O_3. It is evident that the uranium removal efficiency is proportional to the fluorine contents in hematite, highest for 30% F-α-Fe_2O_3 (1.21%, as measured by XPS). The higher removal efficiency in 30% F-TEDA may be attributed to availability of more fluorine for uranium adsorption at surface (schematic Figure 5.11)

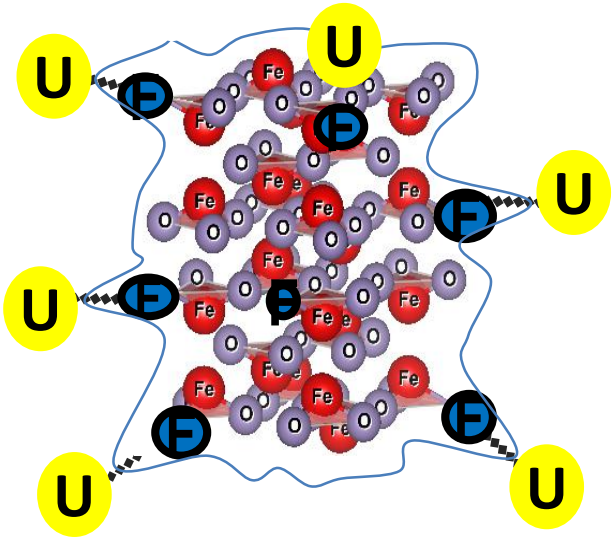

Figure 5.11: Schematic of fluoride assisted uranium adsorption at F-α-Fe_2O_3 surface

The fluorine amount in 0 % to 40 % F-TEDA [Janu et al., 2018] samples and uranium removal efficiency is present in table 5.2.

Table 5.2: Amount of Fluorine versus uranium removal efficiency

S.No.	Sample	Content of Fluorine (by XPS)	U(VI) removal efficiency
1.	Pristine α-Fe_2O_3	0%	31%
2.	10% F- α-Fe_2O_3	ND	38 %
3.	10% F- α-Fe_2O_3	0.41 %	51%
4.	10% F- α-Fe_2O_3	1.21 %	61%
5.	10% F- α-Fe_2O_3	1.13 %	55%

The TEM images are shown in Figure 3.3 (Chapter 3) indicated that shape and morphological modification also improve uranium uptake capacity in comparison of pristine. It is noteworthy that 10% F-TEDA has significant effect on shape where hematite leaf converts towards flower, lead to higher uranium uptake despite undetectable fluorine. At 30% F-TEDA, shape turns to spherical with maximum surface fluorine to give highest uranium removal efficiency. As expected, as shown in Table 5.1, surface area reduces as the amount of surface fluorine increase and shows limited impact on uranium removal.

5.3.3 Effect of Initial Concentration of the U(VI) Ions

The effect of initial concentration of the U(VI) ions was carried out by soaking 25 mg of F-α-Fe_2O_3 in a series of conical flasks which contained 50 mL of U(VI) ions solution at definite concentrations (10-100 ppm) and at pH 5. The conical flasks were kept on the shaker at 140 rpm while maintaining the temperature at 25 °C and 1 h equilibrium time. After adsorption, solution was filtered and the residual concentration was determined. Effects of uranium concentration on removal of uranium by F-α-Fe_2O_3 at temperature 25 °C is presented in Figure 5.12.

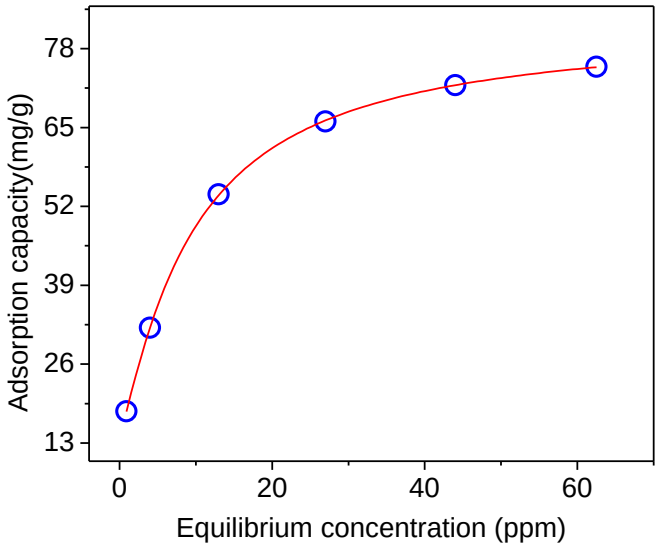

Figure 5.12: Effect of initial uranium concentration on adsorption capacity

The amount of uranium adsorbed per gram of F-α-Fe_2O_3 increased with increase in uranium concentration and then reached the saturation, which is the equilibrium capacity. This is because the increased interaction of U(VI) ions with adsorbate by increasing the initial uranium (VI) concentration while keeping the same mass of adsorbent. The maximum adsorption capacity was experimentally found to be 78 mg/g.

5.3.4 Effect of Contact Time (Adsorption Kinetics)

The contact time experiments were performed at pH 5 by shaking 25 mg F-α-Fe_2O_3 with 50 mL U(VI) ions solution in each flask. The contents of the conical flask were agitated on a shaker at 140 rpm at 25°C varied from 10 minutes to 03 hrs. After adsorption the solution was filtered for analysis of residual U(VI) ions concentration.

The adsorption of U(VI) onto F-α-Fe_2O_3 may be described as a function of the contact time as shown in Figure 5.13.

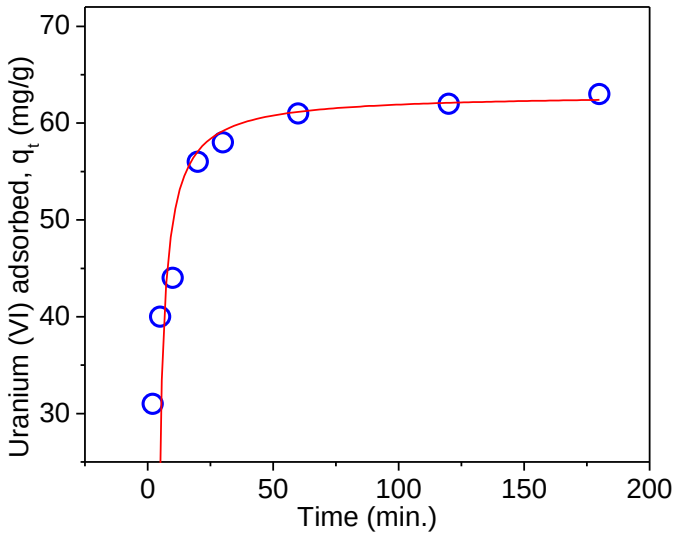

Figure 5.13: Adsorbed amount of U(VI) at different time, volume 50 mL, 50 ppm adsorbent

The U(VI) adsorption increased with time and 95% of the adsorption occurred within 60 min. Any further increase in contact time has a negligible effect on U(VI) adsorption. Therefore, a contact time of 60 min was chosen to approximate equilibrium. The adsorption is higher in the beginning due to the greater number of free sites available for the adsorption of U(VI) ions.

Two types of equations are commonly used to represent the adsorption kinetics. The pseudo first order corresponds to a diffusion-controlled process, is the intra particle diffusion equation[Rudzinski and Plazinski, 2007]. The pseudo first-order kinetic model is given as:

$$\ln(q_e - q_t) = \ln q_e - k_1 t \qquad (5.4)$$

Where, q_e is the amount of metal ion sorbed at equilibrium, q_t is the amount of U(VI) ion on the surface of adsorbate at time t and K_1 is the rate constant of pseudo-first-order adsorption. In case of pseudo-first-order, very low correlation coefficient values were obtained. Therefore, pseudo first order model was not considered for further study.

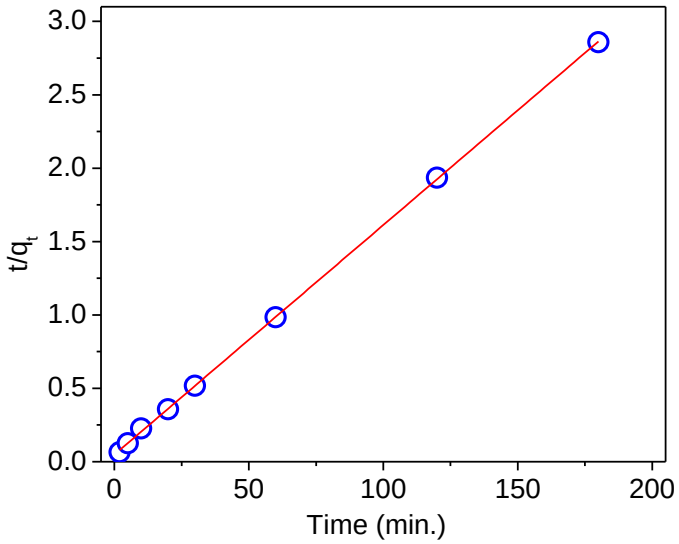

Figure 5.14: Pseudo-second-order kinetic plot of U(VI) adsorption

The second one, pseudo second order is based on solid phase sorption [Ho and McKay, 1999]. The pseudo second-order kinetic model is given as:

$$\frac{t}{q_t} = \frac{1}{k_2 q_e^2} + \frac{t}{q_e} \qquad (5.5)$$

Where, K_2 (g mg^{-1} min^{-1}) is second order rate constant. The plot of t/q_t versus t is presented in Figure 5.14. Parameters of the pseudo-second-order kinetic model were estimated from the experimental data using a linear curve fitting procedure and the results are presented in Table 5.3.

Table 5.3: Kinetic parameters of U(VI) adsorbed onto F-α-Fe_2O_3

Kinetic model	
Pseudo-second-order	Value
K_2(g $mg^{-1}min^{-1}$) $q_{e(cal)}$ (mg/g) R^2	0.05 64 0.99

The pseudo-second-order plot is linear with correlation coefficient of 0.99. Therefore, adsorption behavior may involve valency forces through sharing of electrons between metal ion and adsorbent.

5.3.5 Adsorption Isotherm

The adsorption isotherm indicates about the distribution of adsorbent molecules between the liquid and the solid phase at an equilibrium state. The Langmuir and Freundlich models are generally used to describe equilibrium adsorption isotherms. Figure 5.15a and 5.15b represents Langmuir and Freundlich adsorption isotherms respectively.

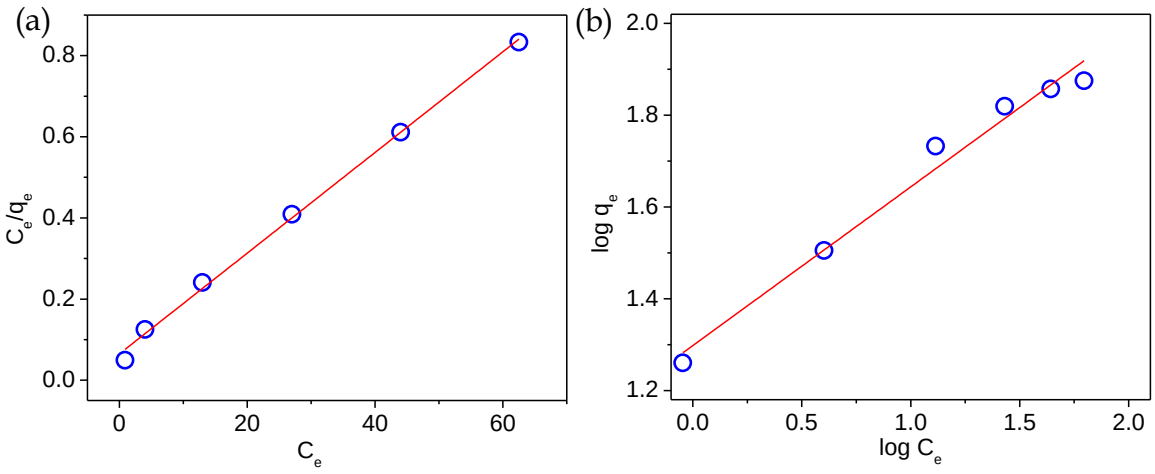

Figure 5.15: (a) Langmuir and (b) Freundlich adsorption of U(VI) onto F-α-Fe_2O_3

Langmuir adsorption isotherm:

Langmuir-type adsorption is considered to be a monolayer process. The maximum adsorption capacity per unit adsorbent mass is determined along with the Langmuir constant showing the solute affinity to the adsorbent. It assumes that there is no interaction between adsorbate and adsorbent. The Langmuir isotherm considers adsorbent surface as homogeneous with identical sites in terms of energy. Its assumptions of monolayer formation and no interaction of adsorbate and adsorbent fail in number of cases limiting its usage. Equation below represents the Langmuir isotherm:

$$\frac{C_e}{q_e} = \frac{1}{Q_o b} + \frac{C_e}{Q_0} \quad (5.6)$$

Where b is a constant of adsorption equilibrium (L/mg) and Q_0 is the saturated monolayer adsorption capacity (mg/g). A linearized plot of C_e/q_e against C_e gives Q_0 and b.

Freundlich adsorption isotherm:

The Freundlich adsorption isotherm is a curve relating the concentration of solute on the surface of adsorbent to the concentration of solute in solution. Freundlich type adsorption is considered to be a multi-layer process in which the amount of adsorbed solute per unit adsorbent mass increases gradually. Freundlich Isotherm correctly established the relationship of adsorption with concentration at lower values. However, it failed to predict value of adsorption at higher concentration.

The empirical form of Freundlich equation based on adsorption on a heterogeneous surface is given as follows:

$$q_e = K_f \times c_e^{1/n} \quad (5.$$

This expression can be linearized to give:

$$ln\mathrm{q_e} = ln\mathrm{K_f} + \frac{1}{\mathrm{n}} ln\mathrm{c_e} \quad (5.8)$$

Where, K_f and n are Freundlich constants, which represent adsorption capacity and adsorption intensity, respectively. K_f and n can be determined from a linear plot of lnq_e against lnC_e [Chung et al., 2015].

Table 5.4 shows the calculated results of the Langmuir and Freundlich isotherm constants. It is found that the adsorption of uranium (VI) on F-α-Fe_2O_3 correlated better with the Langmuir equation (R^2 = 0.99) as compared the Freundlich equation (R^2 = 0.97) under the concentration range studied. Therefore, Langmuir model is relatively more suitable for adsorption equilibrium of uranium (VI) onto F-α-Fe_2O_3 indicating the homogeneous nature of F-α-Fe_2O_3 by monolayer adsorption [Yi et al., 2018]. Further, the Langmuir parameters given in Table 2 can be used to predict about the favorable characteristics of adsorption system using the dimensionless separation factor R_L. The separation factor is given by [Bhatnagar and Jain, 2005].

$$\mathrm{R_L} = \frac{1}{1+\mathrm{bC_0}} \quad (5.9)$$

Where, b is the Langmuir adsorption constant (L/mg) and C_0 is the initial uranium (VI) concentration (mg/L). The values of R_L, shown in Table 2, are ranged from 0.05 to 0.34 for U(VI), hence the adsorption of uranium ions by F-α-Fe_2O_3 could be considered as favorable [Bayramoglu and Arica, 2016]. Based on the Langmuir sorption model, the estimated maximum adsorption capacity using F-α-Fe_2O_3 adsorbent was 79 mg/g for U(VI), exhibiting good agreement with the experimental value 78 mg/g. To the best my knowledge this is maximum uranium removal capacity of hematite/modified hematite observed in literature at 60 min equilibrium time (Table 5.5). The increased capacity of hematite as uranium removal is attributed to additional and strong complexation with surface bonded fluorine.

Table 5.4: Langmuir, Freundlich isotherm model constants and correlation coefficients

Isotherm Model						
Langmuir model				*Freundlich model*		
Q_o *(mg/g)*	*b (L/mg)*	R^2	R_L	K_f	*n*	R^2
79	0.19	0.99	0.05-0.34	20	2.89	0.97

Table 5.5: Literature survey of uranium removal using hematite/ hematite composite

S.No.	Material Used	Achievement	Literature reference
1.	Synthetic hematite sol	Adsorption capacity 3.36 mg g^{-1} at 293K. Equilibrium time: 6 hr. Highest adsorption at pH 7	[Shuibo et al., 2009]
2.	Hematite sol ; prepared by hydrolysis at 100°C of ferric chloride for about 24 h	Adsorption Capacity: 21.17 mg g^{-1} Highest adsorption at pH 6.2	[Ho and Doern, 1985]
3.	Goethite, FeO(OH), prepared from $Fe(NO_3)_3.9H_2O$ and NaOH	Sorption of U(VI) is pH dependent and it increases from 0 to 100% over pH range of 2.5-4.5 Effect of phosphate, carbonate and fulvic studied on adsorption	[Guo et al., 2009]
4.	Nano scale hematite prepared by $Fe(CO)_5$; aerosolized using N_2 gas and decomposed in air at 1000°C-1200°C in furnace	Adsorption affinity decreased as the particle size increased from 12 to 125 nm Achieved 100% adsorption at 1 ppm and 80% at 100 ppm	[Zeng et al., 2009]
5.	Bacteriogenic iron oxides (BIOS) produced by oxidation of iron using Gallionella ferruginea	The maximum adsorption capacity of B IOS was 9.25 mg g^{-1} at 0.1mM carbonate concentration and decreased to 6.93mg g^{-1} at 0.5mM carbonate concentration	[Katsoyiannis, 2007]
6.	Hematite particles synthesized from condensed ferric hydroxide gel	Adsorption Capacity: 8 mg g^{-1} Equilibrium time: 05 hrs.	[Zhao et al., 2012]
7.	Fluorinated hematite	Adsorption capacity: 79 mg g^{-1} Equilibrium time: 01 hrs.	This work

5.4 CONCLUSION

The results indicated that the adsorption capacity of F-α-Fe_2O_3 was affected by the pH, contact time and initial concentration of uranium. The optimal adsorption of uranium was achieved at pH 5. The Langmuir and Freundlich adsorption models were used for a mathematical description of the adsorption equilibrium and Langmuir model fitted better in the studied concentration range. The adsorption capacity of F-α-Fe_2O_3 was found excellent (Langmuir q_m= 79 mg/g) as compared to pristine hematite/ hematite composite. The maximum uranium removal is concomitant with presence of fluorine in F-α-Fe_2O_3. Therefore, fluorine assists for adsorbing uranium at F-α-Fe_2O_3 surface irrespective of changes in surface area. The equilibrium was achieved within 1h time. FTIR, EDX, and XPS analyses confirmed the presence of uranium onto F-α-Fe_2O_3.Therefore, there is good potential to use F-α-Fe_2O_3 for uranium removal for large scale applications.